Capstone title: Controlling the Morphology of Hybrid Organic-Inorganic Lead Bromide Perovskite Films on Planar Substrates

Student name: Haralds Āboliņš

Student number: 10443606

Major: Science

Name supervisor: Dr. F.R. Bradbury

Name reader: Prof. Dr. R. Griessen

Name tutor: Dr. F.M. Scott

Capstone Thesis submitted in partial fulfilment of the requirements for the degree of Bachelor of Science

Date (27-05-2015):

Word count: 10 721

Layman's Summary

The development of sustainable and low-cost alternative energy sources to replace fossil fuels is one of the biggest challenges humanity faces today. There is indisputable evidence that the carbon dioxide released in the atmosphere due to burning of coal, oil and natural gas since the beginning of the industrial revolution is the main reason behind the observed increase in the Earth's surface temperature over the course of the past century. It is widely acknowledged that, in order to prevent dangerous climate change, the increase in the mean surface temperature of the Earth should not exceed 2°C. To meet this target, drastic and immediate reductions in global carbon emissions are necessary.

There are various alternative sources of energy that can be used for developing a carbon neutral economy, but none can compare to solar energy in terms of untapped potential. The Earth receives more energy from the Sun in an hour than the entire human population consumes in a year. Nevertheless, despite the rapidly falling prices of silicon-based solar cells, energy from the sun remains considerably more expensive than fossil fuels in most regions in the world.

In recent years there have been two main thrusts in the solar cell research community - the development of devices made from high quality materials with increasingly higher efficiencies, and the development low cost alternatives that are relatively quick an easy to produce. This divide exists mainly because there has always been a significant trade-off between improving efficiencies and lowering costs. A major step towards an alternative that could combine both of these objectives was made in 2009, when the first solar cells based on a class of materials called perovskites were first developed. Since then perovskite solar cells have experienced an unprecedented rate of improvements in efficiency, which has risen from only 4% in 2012 to 20% today, rivaling even well established commercial solar cells.

One of the fundamental limitations to further efficiency improvements for perovskite solar cells, however, has been a lack of adequate control over the film quality of these materials. The purpose of this study wast thus to develop new deposition methods with better control over the perovskite crystal formation process. It was found that attaching a very thin layer of

long organic molecules to the surface on which the perovskites were to be deposited yielded improved film quality with reproducible results. It was further shown that even better crystal layers could be obtained by adding a chemical called toluene during the deposition process, as well as by performing a second deposition on top of a pre-made perovskite film. To the best of the author's knowledge, the methods developed during this study have not been reported previously, and could have potential applications for both the study of the fundamental properties of perovskites as well as integration of these materials in devices for solar energy conversion.

Abstract

Hybrid organic-inorganic metal halide perovskites have recently emerged as one of the most promising new materials for photovoltaics. They combine the ease of fabrication of organic solar cells with the charge transport properties of inorganic semiconductors, and over a period of only five years perovskite-based solar cells have reached efficiencies of up to 20.1%. To a large extent, these rapid increases in efficiency have been due to improvements in the quality of the perovskite films in terms of surface coverage and crystal size. However, for the planar heterojunction device architecture - the simplest, and likely most commercially scalable design for perovskite solar cells - obtaining good control over film morphology remains a significant challenge, inhibiting both device performance and the investigation of fundamental material properties. Thus, for this study, surface silane-functionalization of planar substrates was employed to improve perovskite film uniformity with controlled crystal size and reduced surface roughness. Bromide perovskites were chosen in particular due to their potentially significant role in the fabrication of low-cost high-efficiency tandem solar cells using perovskites. It was found that the addition of hydrobromic acid to the perovskite precursor solution significantly improved nucleation density on functionalized surfaces, which could be increased further by promoting faster crystallization. Thin, continuous and relatively smooth films could thus be obtained by dripping a non-solvent onto the sample during spin-coating to induce rapid crystal formation. Control over final film thickness and crystal size could be achieved by sequential deposition using a saturated precursor solution, resulting in further growth templated by the first layer of perovskite.

Table of Contents

List of Tables

List of Figures

List of Appendices

Acknowledgements

1   Introduction

In recent years hybrid organic-inorganic metal halide perovskites have been one of the most talked about trends in solar cell technology, mainly due to their unprecedented performance improvements over a very short period of time. It has been only five years since the beginning of widespread research on perovskite photovotaics, yet their efficiencies have soared to 20.1%, rivaling those of more conventional bulk and thin film technologies [1]. Solar cells made from perovskites possess the benefits of being light weight, low cost and easy to fabricate with simple solution or vapor processing techniques [2]. Moreover, the tuneable band gap of these materials makes them ideal candidates for affordable thin-film tandem solar cells, which can reach extremely high efficiencies, but so far have been restricted only to certain niche markets such as the aerospace industry due to high material and production costs [3].

Perovskites possess a range of optical and electrical properties that make them attractive for photovoltaic applications. Their charge carrier mobilites and carrier diffusion lengths are significantly higher than those that of organic films and colloidal quantum dots used to make solar cells, and are comparable to those of $CdTe$ and polycrystalline silicon - the currently most widely used materials for thin film photovoltaics along with $GaAs$ [4] [5]. Perovskites also have been shown to exhibit high carrier lifetimes (up to 2 μs), which are similar to those in $GaAs$, and photoluminescence efficiencies up to 70% [6] [7]. Thus non-radiative recombination in these materials is relatively low, supporting high open-circuit voltages. Consequently, if film thickness and morphology can be optimized, for maximum absorption, with limited losses in charge carrier transport and extraction, high device efficiencies can be expected. Nevertheless, such optimization requires a good understanding of the fundamental properties of the material, which is an active area of research for hybrid organic-inorganic perovskites.

One of the largest limitations for the theoretical understanding, and thus performance, of perovskite photovoltaics is the lack of adequate control of the material's morphology and crystal quality. The presence of pinholes and poor crystallinity have often been attributed as the cause of lower device efficiencies and have been a limiting factor for adequate optical characterization of these materials [4] [8]. The

purpose of this study was thus to develop methods for controlling the morphology of perovskite films as necessary for both optoelectronic characterization and device integration. In particular, focus was put on the less well studied bromide-based perovskites, due to their relatively high (2.2 eV) band gap making them well suited for applications requiring materials with a large open-circuit voltages such as water splitting for solar fuels and, particularly, tandem solar cells. The perovskites were also deposited specifically on planar substrates, which represent the simplest, and, arguably, most easily scalable solar cell design for these materials, and also makes them well suited for optical characterization.

2 Theoretical Background

2.1 Essentials of Surface Chemistry

Here a brief summary is provided of classical nucleation theory and the surface chemistry basics relevant for the following discussion. As for all spontaneous processes at fixed temperature and pressure, for the nucleation of a crystal the Gibbs free energy (G) of the system must decrease. The change in G for homogeneous spherical particle growth from solution is defined by

$$\Delta G_{homogenous} = \Delta G_{bulk} + \Delta G_{surface} = -(\frac{\frac{4}{3}\pi r^3}{\Omega})kTln(\frac{C}{C_0}) + 4\pi r^2\gamma, \qquad (1)$$

where r is the radius of the particle, Ω is the atomic volume of the condensed phase of the nucleating material, k is the Boltzmann constant, T is the temperature of the system, C is is the concentration of the solution, C_0 is the equilibrium concentration, and γ is the surface tension of the particle [9]. The first term in equation 1 defines the change in free energy from the formation of the bulk condensed phase of the system; it increases with higher T and becomes negative only at supersaturated concentrations, when $C > C_0$. The second term defines the change in free energy for the formation of a surface, which is always positive. Thus nucleation and growth of the particle will only occur above a critical particle size (r^*) with an activation energy of ΔG^*, at which $\frac{\Delta G_{bulk}}{\partial r} > \frac{\Delta G_{surface}}{\partial r}$, as shown graphically in figure 1.
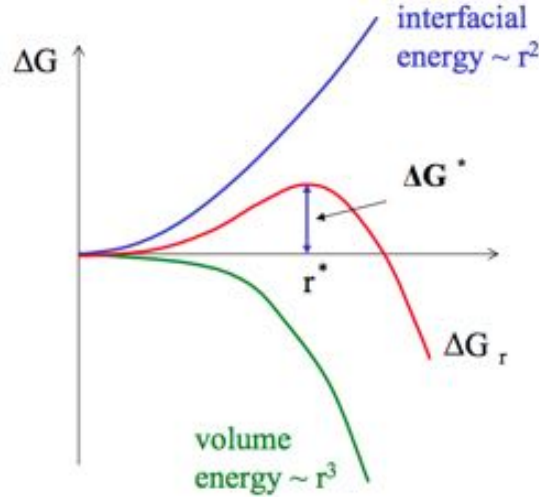
Figure 1: *Free energy diagram for homogeneous particle nucleation and growth. Here r^* is the critical particle radius and ΔG^* is the activation energy for nucleation [10].*

The activation energy is also essential for determining the rate of nucleation (R_N), which is proportional to the probability that a thermal fluctuation will be large enough for nucleation to occur [9]:

$$R_N \sim exp(\frac{-\Delta G^*}{kT}).\tag{2}$$

Thus even small changes in the supersaturation concentration (C), and thus also ΔG_{bulk}, or surface tension (γ) will have a significant effect on on the rate of nucleation, since

$$\Delta G^* \sim \frac{\gamma}{\Delta G_{bulk}^2}\tag{3}$$

For heterogeneous nucleation on the surface of a substrate, instead of just one relevant surface energy term in the free energy equation there are three:

$$\Delta G_{heterogenous} = -(\frac{\frac{4}{3}\pi r^3}{\Omega})kTln(\frac{C}{C_0}) + A_{LS}\gamma_{LS} + A_{SC}\gamma_{SC} - A_{SC}\gamma_{LC},\tag{4}$$

where the different surface tension terms are relevant in a corresponding area A, and are defined in figure 2 [10]. Thus if the interaction of the substrate with the particle is favorable enough that

$$A_{SC}\gamma_{LC} \geq A_{LS}\gamma_{LS} + A_{LC}\gamma_{LC} - (\frac{\frac{4}{3}\pi r^3}{\Omega})kTln(\frac{C}{C_0}),\tag{5}$$

layered growth of the nucleating material will occur, since the overall free energy of the system is reduced [11]. Thus higher supersaturation concentrations and lower

surface tension between the substrate and the nucleating particle will result in better surface coverage. If equation 5 does not hold, island growth of the nucleated particles will occur resulting in larger and thicker individual crystals at lower C and higher γ_{SC} [11].
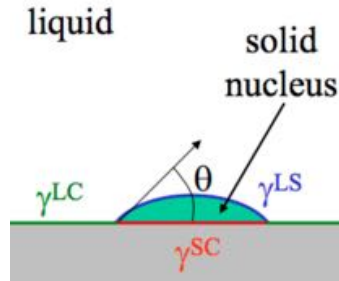
Figure 2: *Diagram of relevant surface tension terms for heterogeneous nucleation [10].*

2.2 Material Description

Metal-halide perovskites are a class of materials with the general formula ABX_3, where A and B are cations that are coordinated by 12 and 6 X anions cuboctahedrally and octahedrally respectively [4] [12]. The resulting three-dimensional structure can be seen in figure 3. Of particular interest for photovloltaic applications are hybrid organic-inorganic perovskites where a methylamonium ($CH_3NH_3^+$) and lead (Pb^{2+}) fill the roles of the A and B cations respectively, and the anion is one of the group VII elements I^-, Br^- or Cl^-. The focus of this study, however, will be specifically on $CH_3NH_3PbBr_3$, which exists in a cubic configuration at room temperature and has a band gap of 2.2 eV. Thus the material cannot absorb photons at wavelengths longer than 550 nm, which is not ideal for single junction solar cells, but can have useful applications for solar water splitting, tandem solar cells and lasing, as only a few examples [13].
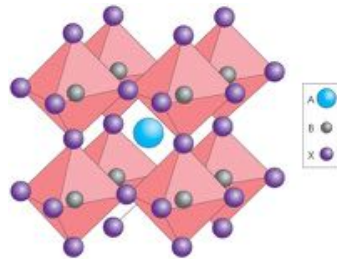
Figure 3: *Crystal structure of an ABX_3 perovskite [14].*

2.3   Current Limitations

It has been demonstrated that planar heterojunction architecture for solar cells made from organic-inorganic metal halide perovskites can offer considerable benefits in terms of device performance and scalability over mesoporous structures, including larger average crystal size, improved carrier mobilities and simplicity; however, control over the film's morphology in these structures remains a significant challenge [8]. Perovskite morphology has often been correlated with device efficiencies and affects multiple optoelectonic properties of these materials [2]. One of the most alarming problems is the presence of pinholes in the perovskite films, which can act as current pathways reducing shunt resistance in the device and thus lowering its open circuit voltage and fill factor, as well as reduce the projected surface area of the device lowering absorption [15]. Moreover, additional losses can be attributed to charge accumulation in trap states at grain boundaries. The passivation or reduction of these surface states with PbI_2 or solvent annealing respectively has been shown to improve PL lifetimes and device efficiency [7] [16] [17]. The exact role of grain boundaries in affecting device performance, however, is yet to be thoroughly explored [4].

Currently rather little is known about the optical properties of perovskites. This is largely due to the high surface roughness of these materials, which creates measurement artifacts during optical characterization, and which cannot be systematically accounted for due to limited control over surface structures [4] [18]. An additional complication is created by the dependence of certain optical parameters, such as the absorption spectrum of perovskites, on the substrate on which the material is deposited. Consequently, reported optical constants have differed considerably on planar substrates and mesoporous templates [19]. The wide variety of these results might be linked to the ratio of amorphous to crystalline material within the films, which is strongly affected by the processing and crystallization conditions [8]. Knowledge of optical parameters such as the dielectric constants and absorption coefficients of the material, however, is critical for gaining a fundamental understanding of the chemical and electrical structure of perovskites. Being able to calculate the absorption and emission properties of these materials would significantly facilitate device integration and optimization as well [4].

2.4 Previous Research

Much of the previous research on the surface morphology of metal halide perovskites has been largely device-oriented rather than focused on the material itself, but has, nevertheless, yielded important insights on the response of perovskite surface structures to different processing parameters. A thorough review of these findings are beyond the scope of this bachelor's thesis, however, some generalized observations will play an important role.

Perovskites can be produced by both solution- and vapor-phase methods [20]. In the most widely used solution-based approach the material is deposited by spin-coating a precursor solution of methylamonium halide and lead halide in a polar solvent onto the substrate, followed by thermal annealing. This is the simplest and very likely the most cost effective method of perovskite processing, and thus the most favorable for commercial scaling. Alternatively, the perovskites can be deposited by co-evaporation of the organic and inorganic precursors [21], or by first spincoating a layer of the lead halide precursor and exposing it to a vapor of the methylamonium halide [16]. These methods have been shown to offer additional control over the morphology of the resulting films; however, they are significantly more time and energy intensive and thus, likely, too expensive to scale up for commercial purposes [22]. Thus deposition via spincoating has most often been the processing method of choice for perovskite photovoltaics, and will also be the approach taken in this study.

The deposition step in perovskite processing is almost always followed by thermal annealing, the precise conditions of which have also been shown to have a siginficant impact on film morphology [20]. In particular, Eperon et al. have shown that film coverage and perovskite crystallization are highly dependent on annealing temperature, duration and inital film thickness before the annealing step takes place [23]. Lower annealing temperatures and higher film thicknesses were shown to correlate well with increased surface coverage and crystal size, and longer annealing times led to more complete crystallization of the perovskites. Xiao et al. have also demonstrated that crystal size and film continuity can be significantly altered through solvent annealing, whereby the perovskite is placed in direct contact with the vapor of a polar solvent during the annealing step, facilitating slow large crystal

formation [17]. However, morphological control via thermal processing will not be the focus of this thesis, and thus annealing conditions will mostly be kept constant. Nevertheless, it is a processing parameter that should not be overlooked, as it could provide a potential route towards further improving the results of this study.

Possibly the most important role in determining the morphology of perovskite films, however, is played by the polar solvents of the precursors. Depending on which solvent or combination of solvents is chosen, a wide array of different surface morphologies can be achieved [4] [8] [12] [20]. Solvents can affect film thickness, crystal size and surface coverage through variations in viscosity, polarity, evaporation rates and the supersaturation precursor concentrations they allow [8] [15] [24]. Very little is currently known about the intermediate configurations that solvents form with the perovskite precursors [4] [20] [25]. Solvent choice has also been successfully used as a tool for controlling the perovskite film structure through solvent engineering [15] [24] [22].

Jeon et al. and Xiao et al. have both developed similar methods for rapidly precipitating out the dissolved perovskites during spincoating to form dense, continuous and reasonably smooth films [22] [24]. The main step in their procedures is the dropcasting of a perovskite non-solvent such as toluene or chlorobenzene during the spincoating process to "force" the perovskite precursors to precipitate. Since Dimethyl sulfoxide (DMSO) was used as the solvent in the approach followed by Jeon et al., the perovskite was not formed immediately upon dripping of the non-solvent. Instead a stable $MAI - PbI_2 - DMSO$ intermediate complex is formed first and only converted to perovskite upon annealing [24]. Xiao et al., on the other hand, used N,N-Dimethylformamide (DMF), which is not known to form any intermediate complexes with the precursors, as the solvent, so a perovskite layer was formed immediately when the chlorobenzene was added [17]. Consequently, the dripping point of the non-solvent played a crucial role in the final film morphology, as can be seen in figure 4. If the clorobenzene was dripped too early, the solution had not yet reached its point of saturation so the induced precipitation was not fast enough for complete surface coverage. If it was dripped to late, nucleation had already occurred and heterogeneous crystal growth had already begun, thus homogeneous surface coverage could no longer be achieved. Thus for the best quality

film the non-solvent had to be added in the narrow window, where the precursor solution is close to supersaturation, but not yet nucleating.
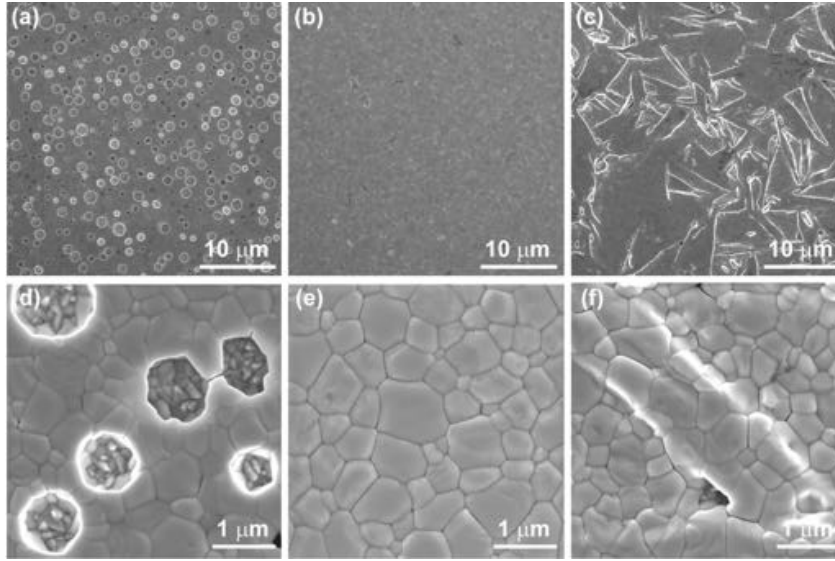
Figure 4: *SEM images of the morphology of a $CH_3NH_3PbI_3$ film spincoated from a precursor solution in DMF with different times of chlorobenzene dripping. Panels show dripping after a,d) two seconds, b,e) four seconds and c,f) eight seconds of spinning [22].*

A largely opposite approach has been taken by Heo et al., who have used hydrobromic acid (HBr) as an additive to the DMF solvent to raise the supersaturation concentration of the perovskite precursors [15]. The higher solubility of the precursors effectively causes the perovskite to crystallize later in the spincoating process when most of the solvent has evaporated, resulting in denser and thinner perovskite films. Nevertheless, they also show that there should be an upper limit to how much HBr can be added to the precursor solution, since it is only at a 48% concentration in water. Heo et al. performed the same experiment using water instead of HBr, and, while the saturated concentration and surface coverage still improved, x-ray diffraction (XRD) analysis showed that the perovskite had partially decomposed back into $PbBr_2$ and CH_3NH_3Br. Frost et al. show that for $CH_3NH_3PbI_3$ in the presence of water decomposition occurs even further into PbI_2, CH_3NH_2 and HI [26]. Lastly, Wang et al. find that, due to this decomposition, the addition of H_2O to the precursor solution inhibits the formation of highly crystalline and oriented films [27].

It has also been shown that the stoichiometry of the perovskite precursors can play

an important role in the film formation process. Multiple research groups have reported improved surface coverage with the addition of excess organic precursor to the precursor solution [28] [29] [30]. Zhang et al. suggest that the improvement arises from a retarded onset of crystallization, which can only proceed once the excess organic component is driven out of the film, resulting in supersaturation of the precursor solution [28]. Yan et al. demonstrate that the excess methylamonium halide in the solution also serves to further dissolve and coordinate (form dipolar covalent bonds around) the lead halide precursor resulting in colloidal intermediates, which ultimately facilitate denser nucleation [30].

Zhang et al. also demonstrate that lead acetate trihydrate ($Pb(CH_3CO_2)_2 \cdot 3H_2O$) substitution for the lead halide in the non-stoichiometric precursor solution can lead to further improvements in film quality and smoothness [28]. Their explanation for this is that driving out excess methylamonium halide from the precursor solution upon drying requires the application of too much heat for too long resulting in coarsening of the resulting perovskite film. However, if lead acetate is used, the compound that needs to be driven out is methylamonium acetate, which is significantly more volatile and thus can be evaporated out more rapidly and at lower temperatures, resulting in dense and uniform films.

Self-assembled monolayers (SAMs) have been used previously by multiple research groups for interfacial engineering to improve extraction of n-type carriers, but none have focused on using SAMs specifically for improving the morphology of the resulting perovskite films [2] [13] [31] [32]. Moreover none of these studies have been on smooth planar substrates, but rather on mesoporous TiO_2 or planar ZnO of unreported roughness. Nevertheless, Zuo et al. and Ogomi et al. reported improved wetting and surface coverage on amino-functionalized substrates of ZnO and TiO_2 respectively. The purpose of this thesis is to further investigate how surface silane-functionalization with amine or thiol terminal groups on planar glass and silicon substrates could help improve and control the morphology of $CH_3NH_3PbBr_3$ films. Silanes are a particularly attractive option for this purpose, since they can relatively easily be deposited on any surface that can be hydroxyl-terminated. It is suspected that amine functional groups will enhance substrate-perovskite interaction by substituting one of the methylamonium cations in the perovskite crystal

structure. The same hypothesis is made by by Zuo et al., as shown in figure 5 [2]. For thiol-functionalized substrates the expectation is that the mercapto (HS) terminal groups will bind to the lead in the perovskite crystal matrix. Nevertheless, both of these interactions are only hypotheses and remain to be tested experimentally.
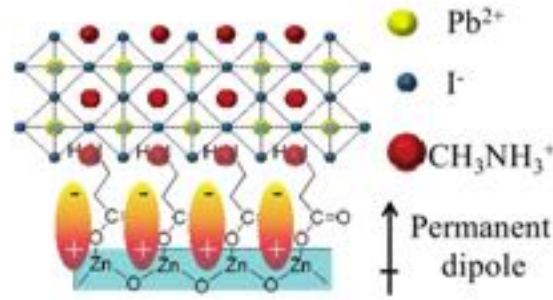
Figure 5: *Interaction of amine functional groups with the perovskite lattice as proposed by Zuo et al. The amines are shown replacing the nearest organic cations of the $CH_3NH_3PbBr_3$ crystal [2].*

3   Methods[1]

3.1   Surface Silane Functionalization

Three types of substrates of roughly the same size (15×15 mm) were used for this study - smooth glass, plasma etched glass, and monocrystalline, polished n-type silicon. Identical procedures were followed for the surface functionalization of the smooth glass and silicon, with one extra plasma treatment step for the etched glass indicated further. Before functionalization the samples had to be cleaned from all organic conaminants on the surface. They were first sonicated in acetone using a Branson 5210 ultrasonic bath for 2 minutes, rinsed with isopropanol, dried under an N_2 stream, then transferred to a 1:1 solution of deionized (DI) water and 37% hydrochloric acid (HCl) and left to sit for 30 minutes. The substrates were subsequently rinsed with DI water and isopropanol, and dried under a stream of N_2. Lastly, to remove the remaining contaminants from the surface and to make it hydroxyl-terminated for funtionalization, the substrates were plasma treated using

---

[1]All chemicals used in this study were purchased from Sigma-Aldrich.

an Oxford Plasmalab 80+ ion beam plasma etcher, by exposing them to an O_2 plasma at 50 W for 2 minutes. For the etched glass substrates an extra step with a plasma of CHF_3 and Ar at 200 W for 10 minutes was used, followed by another iteration of the first step for hydroxyl-termination.

For best results the substrates were silane functionalized immediately after the plasma treatment. The silanes used were: 95% (3-Mercaptopropyl)trimethoxysilane (MPTS) and 99% (3-Aminopropyl)trimethoxysilane (APTMS). Both solution- and vapor-phase functionalization was attempted. For the solution-based approach the substrates were immersed in a solution of 50 ml isopropanol, 500 μl deionized water and 500 μl of the corresponding silane. For optimal results the samples were left in solution for 24 to 48 hours. The substrates were then rinsed with isopropanlol, dried under a stream of N_2, and annealed for 10 minutes at 105°C on a hotplate. For the vapor-phase functionalization 500 μl of the silane was filled into a plastic vile-cap and placed at the bottom of a desiccator. The plasma treated substrates were then distributed on top of a punctured ceramic plate fixed in the middle of the desiccator. The chamber was then sealed with grease and evacuated using a Welch WOB-L 2522 pressure pump. The best quality of functionalization was obtained when the samples were kept in the low-pressure desiccator environment for 48 hours or longer. The perovskites had to be deposited within 3-5 hours after silanization, before the quality of functionalization began to deteriorate.

3.2   Preparation of Precursor Solution

3.2.1   Synthesis of CH_3NH_3Br

The methylamonium bromide (CH_3NH_3Br) used for perovskite synthesis was made using the following procedure obtained from Sarah Brittman (personal communication, 2015). 20 ml of 33wt% methylamine (CH_3NH_2) was added to a beaker in an ice bath and stirred at 250 rpm using a magnetic stirrer. 29 ml of HBr was then added dropwise to the methylamine for approximately 30 minutes, while continuing to stir. The solution was subsequently left on the magnetic stirrer for an additional 2 hours, making sure to replenish the ice bath, so that the precursors did not evaporate before they could react. The beaker was then removed from the ice bath and heated to 130°C to evaporate the solvents, while continuing to stir.

To recrystallize the CH_3NH_3Br, ethanol heated to 70°C was added as little as possible ($\sim$100 ml) to fully redissolve the remaining powder. The beaker was sonicated until the powder was well suspended and continued to heat at 70°C. When the suspension was fully dissolved the resulting solution was left to cool at room temperature and returned to the ice bath once it had cooled down to precipitate out the CH_3NH_3Br crystals. Lastly, the remaining solvent was poured off and the crystals were dried at 130°C, and stored in a vile sealed with parafilm.

3.2.2 Non-Saturated Solutions

Three main types of non-saturated bromide perovskite precursor solutions were used in this study: 1M stoichiometric precursors in N,N-Dimethylformamide (DMF), 2M soichiometric precursors in Dimethyl sulfoxide (DMSO) and a non-stoichiometric precursor solution in DMF with 3M of CH_3NH_3Br and 1M of lead(II) acetate trihydrate ($Pb(CH_3CO_2)_2 \cdot 3H_2O$) used as the metal precursor instead of $PbBr_2$. The first two were also used with the addition of 48% hydrobromic acid (HBr). For the stoichiometric solutions $PbBr_2$ and CH_3NH_3Br were mixed at the desired molarity to form $CH_3NH_3PbBr_3$ in DMF or DMSO, shaken to break up the larger pieces of the precursors or pre-formed perovskite, and then sonicated for approximately 10 minutes until the precursors were dissolved completely. HBr was added only immediately before spincoating at a 5:1 or 10:1 ratio in a smaller vile, which was shaken before use. For the non-stoichiometric solution, $CH_3NH_3PbBr_3$ and $Pb(CH_3CO_2)_2 \cdot 3H_2O$ were mixed at a 3:1 molar ratio in DMF to form a $\sim$40wt% solution, then shaken and sonicated until the precursors were completely dissolved.

3.2.3 Saturated Solutions

For this study only stoichiometric saturated precursor solutions were used. The same procedure as described in the previous section was followed, except the molarities of the stoichiometric precursors were now 2M and 4.5M for DMF and DMSO respectively, and the resulting mixtures were sonicated for 30 minutes to reach maximum saturation. Since the solutions were intentionally made supersaturated, not all precursors dissolved during sonication and some residual pre-crystallized perovskite powder remained in the viles. Consequently, the solutions were subse-

quently centrifuged using a Hettich Universal 320 centrifuge at 10 000 rpm for 5 minutes for DMF and 10 minutes for DMSO. If HBr was used in saturated solutions, it was added already at the precursor mixing stage at a 10:1 or 5:1 ratio to the polar solvent so that the final solution was still saturated.

3.3 Deposition of $CH_3NH_3PbBr_3$

$CH_3NH_3PbBr_3$ films were deposited using a Polos Spin 151 spincoater, in all cases followed by annealing for 5 minutes at 100°C. Table 1 summarizes the spincoating conditions used for the samples discussed in this thesis.

Table 1: *Spincoating conditions used for samples discussed in this study.*

Solution	Figures	Spin Speed (rpm)	Spin Time (s)	Additional Comments
DMF	6 a,b)	3000	40	-
DMF + HBr	6 c,d); 7 b)	3000	200	-
	7 c)	7000	100	
	7 d); 10; 12 a,b)	10 000	60	
DMF + HBr with Toluene Dripping	15 a,c)	10 000	60	Non-optimal toluene drip time Toluene dripping 1 s before film changes colour for DMF + HBr control sample
	15 b); 16; 17	10 000	60	
DMSO + HBr	9 a,b)	3000	200	-
Saturated	12 d,e); 14	2000	100	Saturated solution dripped dynamically on an already spinning "seed" layer
	13 a)	3000	60	
	12 f); 13 b)	10 000	60	
DMF with $Pb(CH_3CO_2)_2$	11 a,b)	5000	60	-
	11 c,d)	10 000	100	

3.4 Sample Characterization

The most prominent morphological characteristics of each sample were first determined and imaged using a Zeiss Axio Imager.A2m optical microscope. Overall morphology was characterized with bright field imaging, and roughness was checked qualitatively from the amount of scattering using dark field imaging. For morphological features of sub-micron scale a FEI Verios 460 scanning electron microscope (SEM) was used. A Veeco Dimension 3100 atomic force microscope (AFM) in tapping mode was used for surface roughness characterization. Lasty, a Bruker D2 Phaser x-ray diffractometer (XRD) was used to determine the material composition and crystallinity of the resulting perovskite films.

4 Results and Discussion

4.1 Film Morphology on Functionalizied Substrates

The following sections summarize the most important findings on the resulting perovskite film morphologies when deposited on silane-functionalized substrates using different precursor solutions.

4.1.1 Improved Nucleation with Addition of Hydrobromic Acid

Here the possibility of using a $CH_3NH_3PbBr_3$ precursor solution in DMF with added HBr on substrates thiol-functionalized with (3-Mercaptopropyl)trimethoxy-silane (MPTS) is demonstrated as an effective tool for improving perovskite nucleation and crystal faceting. Panels a) and b) in figure 6 show the resulting perovskite crystallites on O_2 plasma treated and thiol-functionalized glass substrates, when deposited from a 1M stoichiometric precursor solution in DMF, respectively. A slight change in morphology could be observed when a functionalized substrate was used, but the crystals remained poorly faceted and with relatively low nucleation density - far from the desired smooth and continuous films. The addition of hydrobromic acid (HBr) to the perovskite precursor solution, however, was found to significantly increase the nucleation density and faceting of the resulting crystals. Generally, better nucleation with added HBr was not surprising, since it increases the solubility of the precursors and thus the supersaturation concentration, lowering the free energy barrier for nucleation, as outlined in the theoretical background. Somewhat less expected was the stark difference in the extent to which nucleation density was improved between non-functionalized and functionalized substrates as can be seen in panels c) and d) of figure 6 respectively. Thus the addition of hydrobromic acid to the precursor solution was in some way facilitating the thiol-perovskite interaction, which had apparently lowered the surface energy of the substrate-crystal interface, making smaller and denser crystallites, which generally have less negative bulk free energies, energetically more favorable.

14
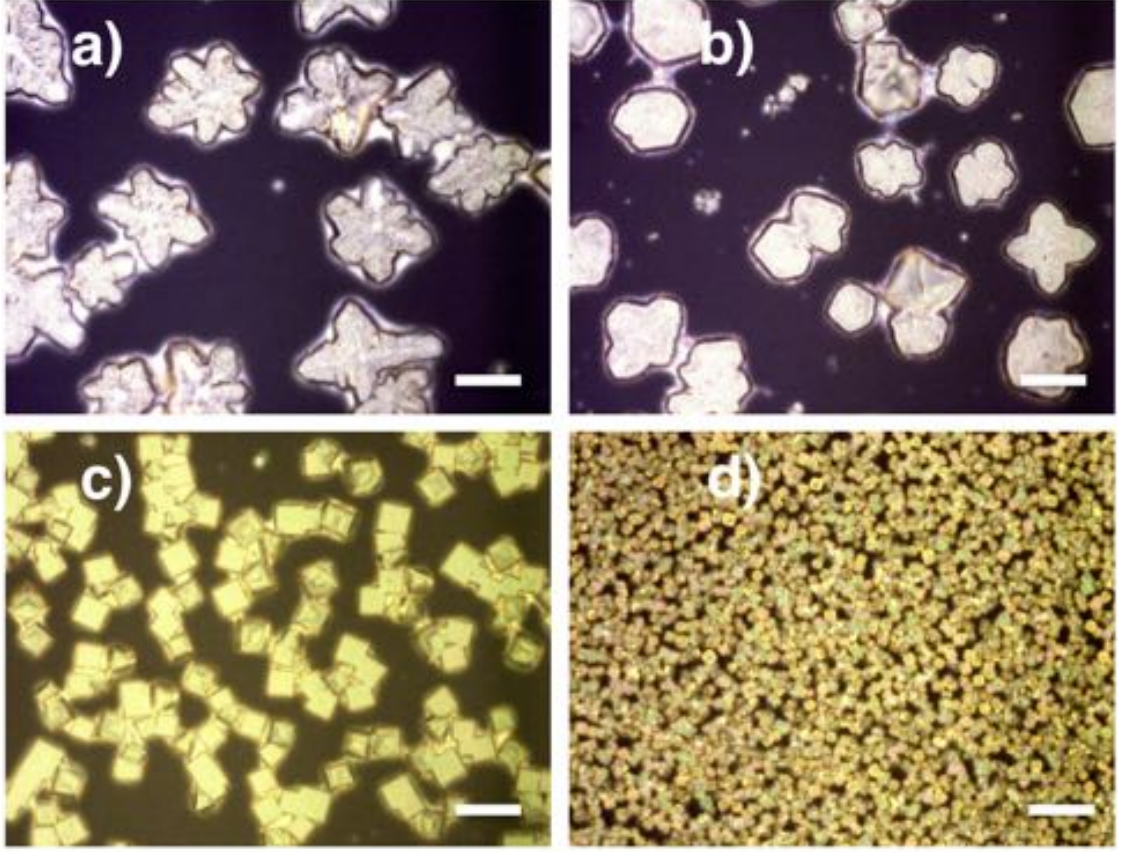
Figure 6: *Bright-field optical microscope images of $CH_3NH_3PbBr_3$ films spincoated on a,c) O_2 plasma treated and b,d) thiol-functionalized smooth glass substrates. Top panels show films deposited from a precursor solution in DMF. In the bottom row images the same precursor solution has been mixed with HBr at a 10:1 ratio. Scale bars - 10 μm.*

Nevertheless, the films were still not continuous, indicating that the bulk free energy term still dominated the lowered surface energy term at the substrate-perovskite interface. Thus the formation of small dense crystallites was a purely kinetic process. This was further demonstrated by increasing spin speed, which yielded even denser nucleation, as shown in figure 7. The color shift of the film from orange to yellow with higher spin speeds indicated that film thickness had increased as well.This was, of course, expected, since the rate of solvent evaporation increases at higher spin speeds, raising the instantaneous supersaturation, and thus facilitating rapid nucleation. The theormodynamicaly more favorable configuration, however, is shown in panel a) of figure 7, where the precursor solution was not spincoated but allowed to dry at room temperature overnight. Note that the scale bar in panel a) is 100 μm, while the rest in figure 7 are 10 μm.

15
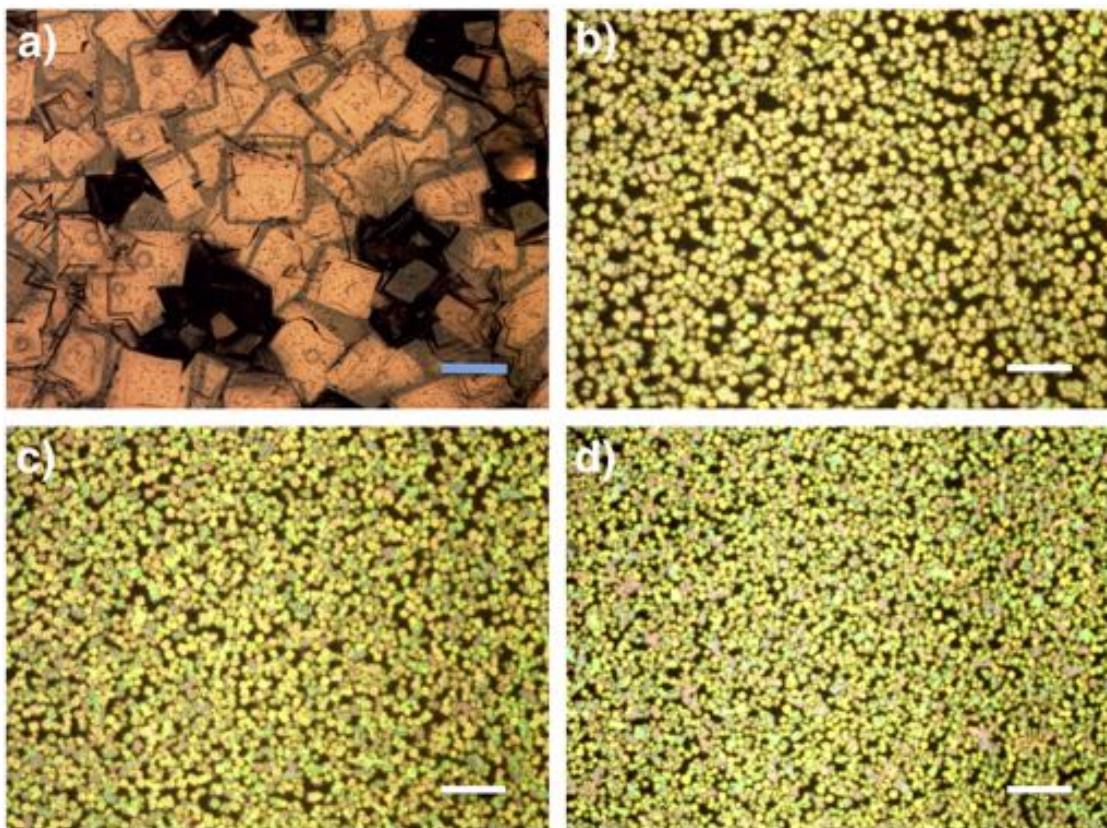
Figure 7: *Bright-field optical microscope images of $CH_3NH_3PbBr_3$ films on thiol-functionalized smooth glass substrates. The film in panel a) was dropcast on the substrate and left to dry overnight. The other three samples were spincoated at a) 3000, b) 7000 and c) 10 000 rpm respectively. Blue scale bar - 100 μm, white scale bars 10 - μm.*

The increase in faceting of the perovskite crystallites after the addition of HBr, however, cannot be explained only by increased supersaturation concentration, particularly at high spin speeds, where the rate of crystallization is increased, and should thus result in less well defined structures. There is some evidence that the addition of hydrodromic acid to the precursor solution could result in the formation of an intermediate complex. Figure 8 a) shows an optical image of a large transparent crystal formed when a saturated perovskite solution in DMF and HBr at a 5:1 ratio was dropcast on an amino-functionalized substrate, covered with a piece of Polydimethylsiloxane (PDMS) and allowed to dry overnight. Figure 8 c) shows an XRD scan of the corresponding sample together with reference patterns for powders of $CH_3NH_3PbBr_3$, $PbBr_2$ and CH_3NH_3Br. The presence of peaks not corresponding to the perovskite or either of the precursors indicates the presence of another, previously unreported, material, possibly an intermediate

complex, formed during the drying of the film. Figure 8 b) shows a picture of similar transparent crystals formed in a saturated perovskite solution in 5:1 DMF and HBr after about a month of sitting. Additional evidence that supports the existence of an intermediate compound is that, when a non-saturated precursor solution with a 5:1 ratio to HBr was made, the film did not turn yellow upon spincoating even after 200 s, indicating that a perovskite layer had not formed, and only did form when the sample was heated. However, perovskites from 10:1 and pure DMF solutions would take no longer than 10 seconds to crystalize at the same spin speed. Wang et al. report that combining lead iodide (PbI_2) and hydroiodic acid (HI) in DMF can result in the formation of ($HPbI_x$) [27]. They suggest that this compound is responsible for the observed reduced crystallization rate of the perovskite, ultimately leading to highly crystaline films. Their rationale is that for the perovskite to form the organic precursor ions would need to intercalate the intermediate PbI_6 octahedral framework to replace the hydrogen bonded H^+ ions, which is a relatively slow process. The results of Wang et al. could thus lead to speculation that the observed intermediate crystals could be $HPbBr_x$ precipitated out of the saturated solutions, but further investigation is needed to confirm this hypothesis.
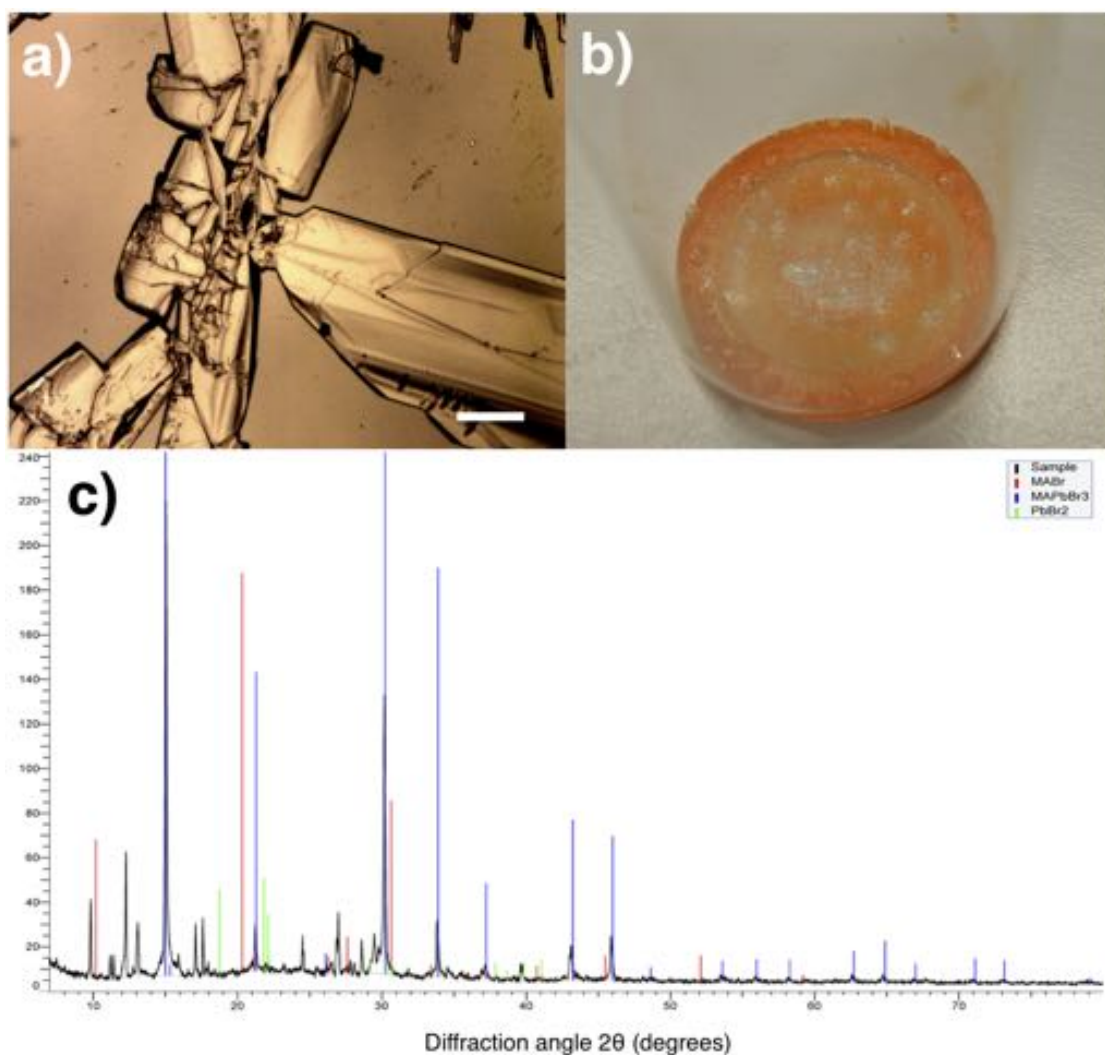
Figure 8: *Potential intermediate complex in bromide perovskite precursor solution in DMF mixed with HBr: a) Optical image of transparent crystal formed after dropcasting a saturated $CH_3NH_3PbBr_3$ precursor solution on an amino-functionalized smooth glass substrate, covering it with a piece of PDMS and leaving to dry overnight (scale bar 100 μm); b) photo of transparent crystals precipitated from the same solution after sitting for approximately a month; c) XRD peaks of the sample in panel a) (black) together with reference peaks of CH_3NH_3Br (red), $CH_3NH_3PbBr_3$ (blue) and $PbBr_2$ (green) powders. Vertical scale is not normalized, and is relevant only in terms of relative peak heights for each material separately.*

4.1.2 Inhibited Substrate-Perovskite Interaction in DMSO

The bromide perovskites were also deposited on thiol functionalized substrates from DMSO. However, the solution would not wet the substrate, and would fly off when spun. Since DMSO has been reported to form and intermediate com-

plex with the lead halide in solution [15], it is possible that interaction between the thiol groups of the silane and the lead are effectively screened, thus limiting the substrate-precursor interaction. Better wetting could be achieved when hydrobromic acid was added to the precursor solution, which was subsequently left to sit for 15 minutes on the substrate before spincoating. In this case, wetting was likely improved due to protonation of the thiols by HBr, makin them charged, and thus improving interaction with the polar solvent. The resulting film can be seen in figure 9 a). Panel b) shows the resulting perovskite film on an etched glass substrate using the same procedure as in a). The green tinting of panel b) is an artifact of the microscope with no physical significance. The similarity between the resulting films on a functionalized smooth glass and non-functionalized etched glass substrates indicates that, although, wetting of the substrate was improved, interaction between the perovskite precursors and the mercapto groups on the substrate are still likely screened by solvent coordination or an intermediate complex.
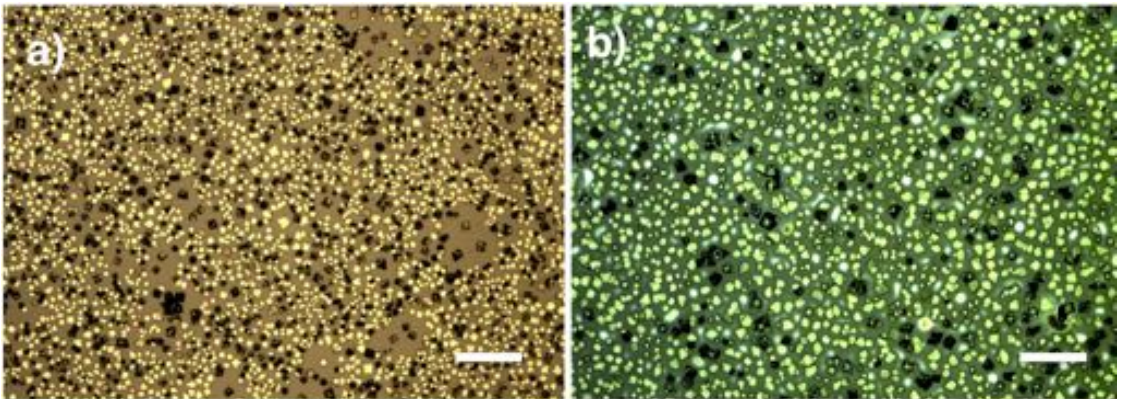
Figure 9: *Bright-field optical microscope images of bromide perovskite films deposited onto a) a thiol-functionalized smooth glass substrate and b) a non-functionalized etched glass substrate from a precursor solution in DMSO mixed with HBr at a 10:1 ratio. The green tint in panel b) is an artifact of the microscope, and has no physical significance. Scale bars - 100 μm.*

4.1.3 Comparing Thiol and Amine Functionalization

As an alternative to thiol-functionalization, surface amino-functionalization with (3-Aminopropyl)trimethoxysilane (APTMS) was also tested. No obvious difference

in the resulting films on MPTS and APTMS could be seen when the perovskites were spincoated from pure DMF solutions. However, when the films were deposited from a solution of DMF with the addition of HBr an increase in crystal density over that on MPTS functionalized substrates could be observed, as can be seen by comparing figures7 c) and 10 a). Thus either the interaction between perovskites and amines is slightly stronger than with thiols, or the packing density of the amino-silanes is somewhat higher than for the mercapto-silanes. Using the amino-functionalized substrates the importance of functionalization time could also more clearly be distinguished. Figure 10 a) shows a perovskite layer obtained on a substrate that was functionalized in a desiccator for more than 48 hours, while in panel b) the functionalization was done for only 20 hours yielding a significantly lower crystal density.
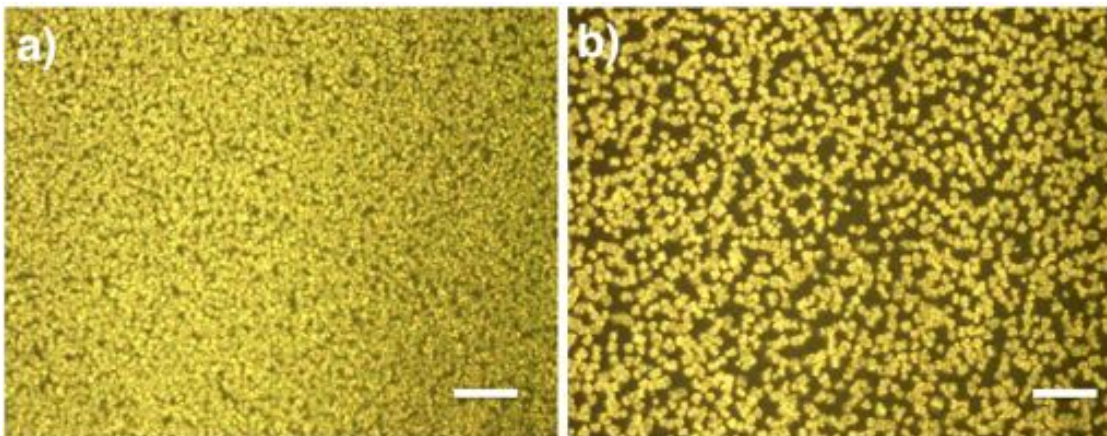
Figure 10: *Bright-field optical microscope images of $CH_3NH_3PbBr_3$ films on smooth glass substrates functionalized with amino-silanes for a) 48 hours and b) 20 hours. Scale bars - 10 μm.*

Comparing figure 10 to figure 7 it can also be seen that the crystals are significantly more preferentially oriented for the thiol-functionalized substrates. This was also shown using x-ray diffraction to check the relative peak intensities or diffraction from different crystal planes. In particular signal from the[100] plane, which is usually dominant in crystals with a cubic lattice structure, was compared to that from the [110] plane. The results were compared to a reference powder of bromide perovkite crystals obtained from Sarah Brittman (personal communication, 2015), and can be seen in Table 2. Both samples show an increase in preferential orien-

tation relative to the reference powder, but the change is much more significant for the thiol-functionalized substrate. The reason for this discrepancy remains unknown, and would likely require the study of the precise interaction mechanism between the amine functional groups and the perovskite crystals.

Table 2: *Relative x-ray diffraction intensities for [100] and [110] planes in $CH_3NH_3PbBr_3$ crystals deposited on thiol- and amino-functionalized substrates from a precursor solution in DMF mixed with HBr at a 10:1 ratio.*

Substrate	Peak Ratio [100]:[110]
Thiol-Functionalized	947:1
Amino-Functionalized	50:1
Reference Powder	9:1

Another difference for amino-funtionalized substrates was that no loading time was necessary before spincoating, and films could be deposited from even a pure DMSO solution, which would not wet the thiol-functionalized substrates. Yan et al. suggest that for stoichiometric iodide perovskite precursor solutions CH_3NH_3I can act as a surfactant for PbI_2 in an intermediate configuration [30]. Thus, if this is also the case for CH_3NH_3Br, improved interaction with amines could be due to the amino groups substituting the similar $CH_3NH_3^+$ anions in some of these surfactants. Additionally, when lead bromide alone was deposited on the substrate from DMF without the organic precursor, very smooth and continuous films could be obtained on thiol functionalized substrates, while very poor coverage resulted on the amines. This is in agreement with the hypothesis that thiols would bind to the lead cations in the perovskites, while amines would replace the organic cations. Nevertheless, a more direct an thorough investigation of the silane-perovskite interactions is necessary to validate the previous statement. For example, Fourier transform infrared or Raman spectroscopy could be used to more precisely characterize the bonding of the perovskite to the functional groups on the surface.

4.1.4   Lead Acetate Precursor for Preferential Crystal Orientation

To further test the difference between thiol- and amino-functionalized substrates a non-stoichiometric $CH_3NH_3PbBr_3$ precursor solution, with the $PbBr_2$ precursor replaced by lead acetate ($Pb(CH_3CO_2)_2$), was used. The resulting films on both types of substrates can be seen in figure 11. One of the most prominent features of these films was the apparent extremely preferential orientation of the crystals. Particularly, when the crystals were deposited at high spin speeds, as in panels a) and b) of figure 11, essentially all crystals were oriented with the top facet parallel to the substrate surface. Judging by the prominent interference fringes seen on the crystals it could also be inferred that the films were significantly thinner (on the order of a few hundred nanometers) than those from stoichiometric solutions with the conventional precursors and added HBr, indicating that crystallization occurred at an even later stage in the spincoating process. This is consistent with the mechanism proposed by Zhang et al., whereby the presence excess organic cations in the film retards the onset of crystallization resulting in a highly supersaturated solution, and consequently dense and thin perovskite layers [28].

Comparing the density of crystallites in panels a) and b) of figure 11, a considerable difference in nucleation density can be seen. The two films were prepared using exactly the same procedure, but on substrates with different functionalizations. In the previous section it was shown that in such cases nucleation was denser on the amino-functionalized substrates, whereas here the opposite was observed. One possible explanation for this could be the coordination of lead precursor complexes by methylamine cations in non-stoichiometric precursor solutions as proposed by Yan et al. [30]. In this mechanism the methylamine intercalates the lead halide matrix only after nucleation, which could be more favorable on thiol-functionalized substrates due to the potentially stronger interaction with the lead cations. Nevertheless, this explanation is purely speculative, and should be verified experimentally.

The bottom row in figure 11 shows the resulting films c) on a substrate with poor functionalizaton and d) spincoated at a slower spin speed. The quality of functionalization was determined from the difference in nucleation density of reference films as in figure 10. Both of these conditions should have thus resulted in less

dense films with larger crystallites, in figures 7 and 10. This is precisely what was observed; however, the growth of the crystals was significantly different on the two substrates. While the crystallites on the thiol-functionalized substrate continued to grow retaining the same cubic shape, the ones on the amino-functionalized substrate seemed to lose symmetry and grow in ribbon-like structures, which are somewhat apparent also in panel b) of figure 11. The precise mechanism driving this asymmetrical growth remains unknown and should be investigated further.
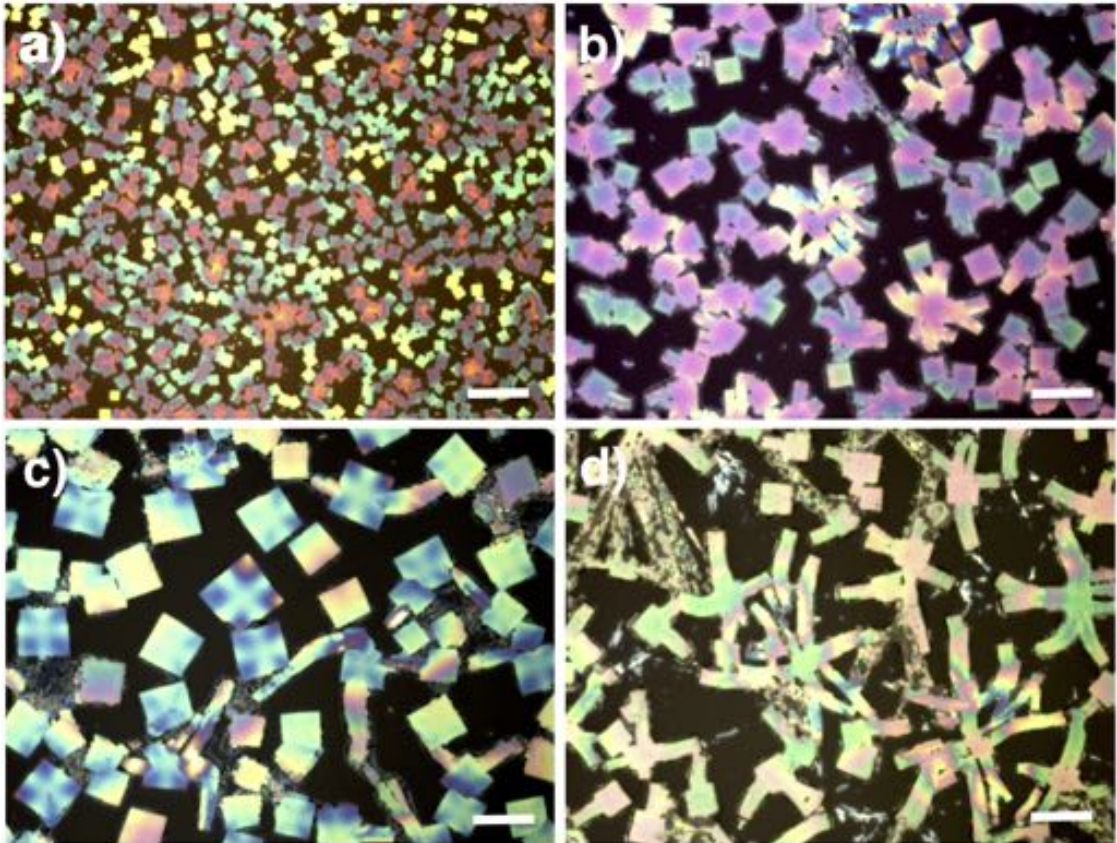
Figure 11: *Bright-field optical microscope images of $CH_3NH_3PbBr_3$ films deposited on a,c) thiol- and b,d) amino-functionalized substrates from a 40wt% non-stoichiometric precursor solution of CH_3NH_3Br and $Pb(CH_3CO_2)_2 \cdot 3H_2O$ in DMF at a 3:1 molar ratio. Films were deposited at 10 000 rpm in panels a) and b). In panel c) the crystals were deposited at 10 000 rpm on a poorly functionalized substrate, while in panel d) they were deposited at 5000 rpm, both with the intention of obtaining lower nucleation density. Scale bars - 10 μm.*

4.2 Controlling Film Morphology with Sequential Deposition

4.2.1 Templating by First Deposition

While the one step deposition methods on functionalized substrates did not yield continuous films of bromide perovskite, it was found that full surface coverage could be achieved by utilizing a sequential deposition method. Here a saturated precursor solution was dynamically dropcast on an already deposited film during a second spincoating step. This yielded continuous films with a morphology resembling that of the starting "seed" layer, but with larger crystallites. It was, however, crucial for the solution to be fully saturated, as it would dissolve the underlying layer even with concentrations just slightly below saturation.

Figure 12 shows the importance of the "seed" layer density, crystal size and orientation for the final film morphology. As can be seen by comparing panels a) and d) to b) and e), fewer and larger crystals in the initial layer would result in larger crystallites in the resulting film as well, which is what would be expected, if the decrease in free energy associated with island growth of the perovskite was larger than for layered growth, since more new material would be grown on each individual crystal. Panels c) and f) in figure 12 show that, if a dense enough initial layer of preferentially oriented crystallites could be deposited, it should also be possible to obtain a relatively smooth and continuous final perovskite layer. Although sequential deposition at slower spin speeds or with different solvents could have improved continuity of the film in panel f) of figure 14, no extensive experiments were conducted on "seed" layers as the one in panel c). It was suspected that the $Pb(CH_3CO_2)_2 \cdot 3H_2O$ precursor necessary for the formation of such layers might be degrading in an oxygen atmosphere, and thus would have to be handled in a glove-box, which was outside the scope of this investigation.
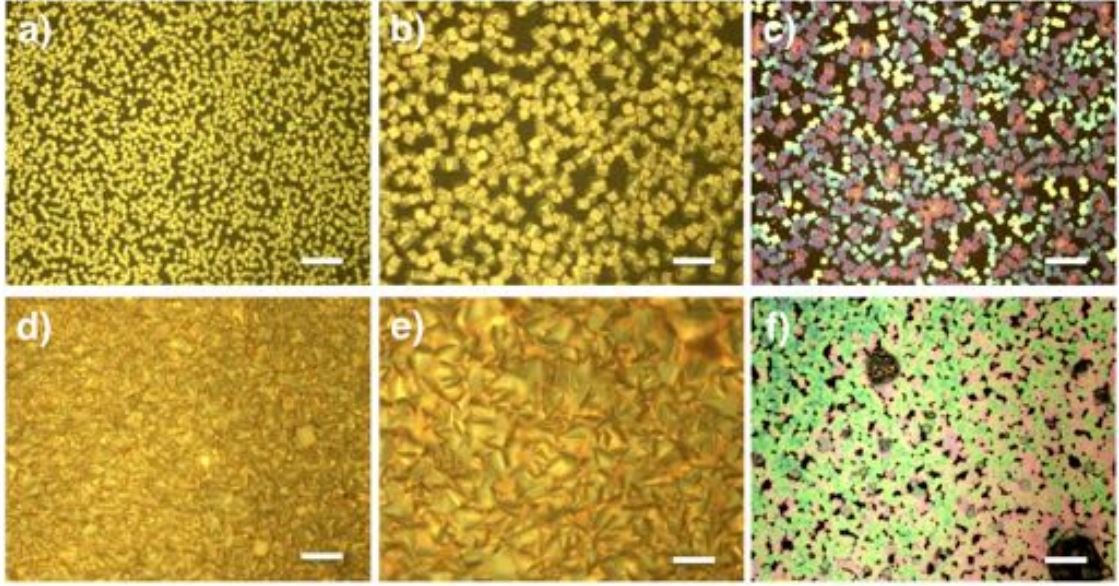
Figure 12: *Bright-field optical microscope images of $CH_3NH_3PbBr_3$ films from sequential deposition on different perovskite "seed" layers. Top row: optical images of $CH_3NH_3PbBr_3$ films deposited on a,b) amino- and c) thiol-functionalized substrates from a) a 1M precursor solution in DMF mixed with HBr at a 10:1 ratio, b) a saturated precursor solution in DMF mixed with HBr at a 10:1 ratio, and c) a non-stoichiometric solution of CH_3NH_3Br and $Pb(CH_3CO_2)_2 \cdot 3H_2O$ at a 3:1 molar ratio in DMF. Bottom row: optical images of saturated $CH_3NH_3PbBr_3$ precursor solutions in DMF with HBr at a 10:1 ratio dynamically deposited on the corresponding substrates seen in the top row during sequential spincoating at d,e) 2000 rpm and f) 10 000 rpm. Scale bars - 100 μm.*

4.2.2 Controlling Crystal Size by Varying Spin Speed and Solvent

The speed at which the second layer was spincoated and the choice of solvent also played an important role for the final film morphology. Panels a) and b) of figure 13 show scanning electron microscope (SEM) images of the resulting perovskite films when a precursor solution of DMF with a 10% addition of HBr was dropcasted on an initial film similar to that of figure 10 a) at 3000 and 10 000 rpm respectively. The film deposited at a slower spin speed exhibited significantly better coverage, yet with only marginally larger crystallite size. Thus the slower crystallization at lower spin speeds could be enabling crystal growth in the voids between the initial crystallites in the "seed" layer in addition to growth on existing crystals. Nevertheless, this might be specific only to precursor solutions in DMF with an HBr additive, as discussed further.
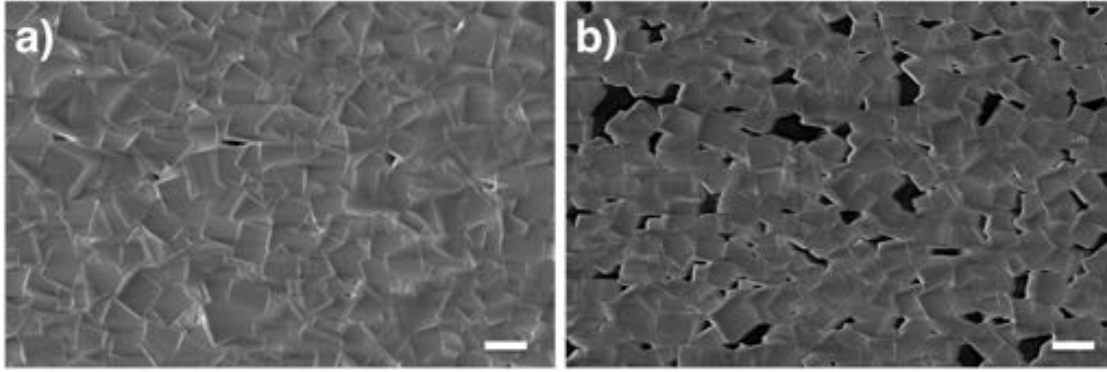
Figure 13: *SEM images of sequentially deposited $CH_3NH_3PbBr_3$ films with the saturated precursor solution in DMF with HBr at a 10:1 ratio dynamically deposited at a) 3000 rpm and b) 10 000 rpm. Scale bars - 500 nm.*

Figure 14 shows SEM images of the resulting films from sequential deposition on a first layer similar to that of figure 10 b) using saturated precursor solutions of plain DMF, DMF with a 20% addition of HBr and DMSO with a 10% addition of HBr for the second step. The sequential layers grown from DMSO with HBr and plain DMF differ considerably from that of DMF with HBr. The growth in figure 14 a) was obviously not solely templated by the first layer. Firstly, the crystal faceting was significantly worse than for any other sample in figures 13 and 14. This this deterioration was likely due to the higher HBr concentration in the precursor solution, which was twice as high as in any of the other samples with added HBr. Consequently there was also a higher concentration of water in the precursor solution, which has been shown to adversely affect film quality [15] [27]. Secondly, contrary to the perovskites grown from a solution of only DMF, for which charging of the exposed underlying glass is clearly visible in the larger white regions in figure 14 b), perovskite had also deposited in the voids between the larger crystals for the DMF solution with added HBr. This indicates that perovskite-substrate interaction might only be strong enough for this to happen when HBr is incorporated into the precursor solution. Such a judgement cannot be made for the DMSO solution with HBr, since all voids were filled solely by templated crystal growth, which was more prominent than for DMF, since crystalization from DMSO is significantly slower. Contrary to large parts on the substrate from panel b) in figure 14, the white regions in panel c) are from crystal edges, not charging glass.
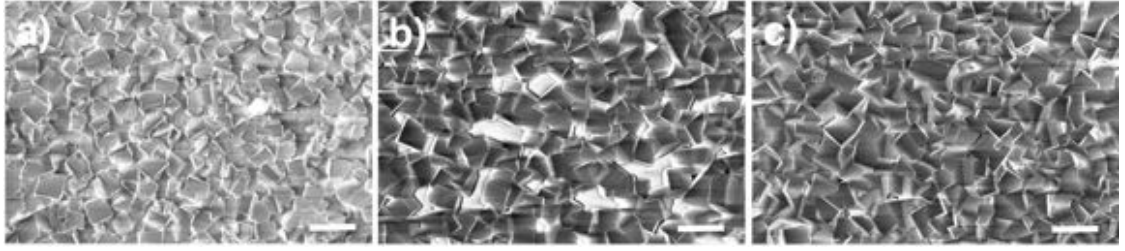
Figure 14: *SEM images of sequentially deposited $CH_3NH_3PbBr_3$ films with the saturated precursor solution deposited from a) DMF with HBr at a 5:1 ratio, b) DMF and c) DMSO with HBr at a 10:1 ratio. Scale bars - 3 μm.*

4.3 Controlling Film Morphology with Addition of Non-Solvent

In section 4.1.2 it was shown for a perovskite precursor solution in DMF with HBr that with increasing the spincoating speed the kinetic barrier for nucleation on the functionalized substrates could be significantly reduced. However, full surface coverage could not be obtained due to the maximum spin speed limitations of the spincoater. To reduce the kinetic barrier further a miscible non-solvent was dripped on the substrate during the spincoating step to force the perovskite to precipitate out of the precursor solution. The method was first described by Xiao et al. using chlorobenzene dripping for iodide perovskite deposition on dense TiO_2, yielding highly uniform surface coverage [17].

4.3.1 Optimizing Time of Dripping

As outlined in the threoretical background section, due to the evaporation and crystallization dynamics during the spincoating step, there is a very narrow window in which non-solvent dripping will yield a perfectly continuous film [17]. This was also confirmed experimentally as can be seen in figure 15. At first, the crystal size decreased and film density increased with a longer delay time before toluene dripping. However, if the non-solvent was added after more than 9 seconds of spinning the average crystal size increased from ∼100 nm to ∼1 μm. This corresponded to the point at which the precursor solution had reached its maximum point of saturation and was forced to nucleate, as determined by the time at which the film changed color from transparent to yellow in a control sample. Thus, if

toluene was dripped after this point, it forced the more rapid growth of existing crystals rather than increased nucleation.
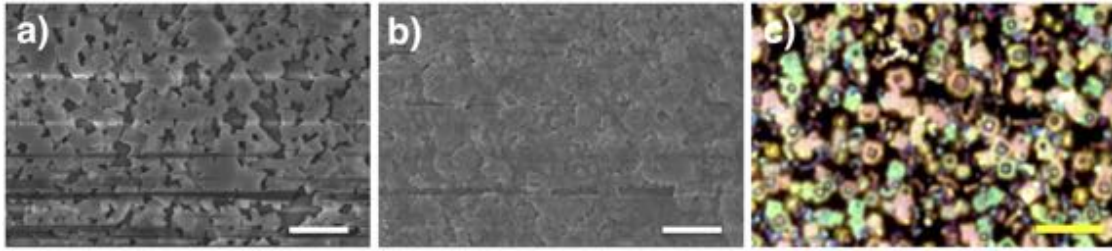

Figure 15: *SEM images and optical image of $CH_3NH_3PbBr_3$ films spincoated on thiol-functionalized substrates from a precursor solution in DMF mixed with HBr at a 10:1 ratio with toluene dripping after a) 6, b) 9) and c)12 seconds of spinning. White scale bars - 1 μm, yellow scale bar - 5 μm.*

4.3.2 Importance of Precursor Concentration and Substrate Material

Film uniformity could be improved further with increased concentration of the precursor solution. Figure 16 a) shows the resulting perovskite film when a saturated solution of DMF with HBr was used. Individual crystallites could no longer be discerned, and, from AMF measurements, surface roughness seemed to be reduced from $\sim$200 nm peak-to-valley variation to $\sim$150 nm. However, there were some apparent measurement artifacts in the image of the rougher sample (see appendix B), thus the reduction in roughness is yet to be reliably verified.

If the perovskite was deposited on an amino-functionalized substrate instead, the morphology of figure 16 b) was obtained, with relatively large domain structures, instead of cubic crystallites as in figure 15. The origin of the small pinholes is unknown, but might be related to the relatively poor amino-functionalization of the substrates, which were left in the desiccator for only 20 hours, which was previously shown to be insufficient for maximum silane density. Lastly, figure 16 c) shows the resulting film on an amino-functionalized silicon substrate. The toluene dripping point was not optimized for this sample, but, interestingly, unlike on glass substrates, the crystallites seem to preferentially orientate at the surface, yielding an apparently rather smooth surface. Thus it seems that on smaller scales the substrate material still has an influence on the final film morphology, despite the surface functionalization. Nevertheless, nucleation densities remain comparable.
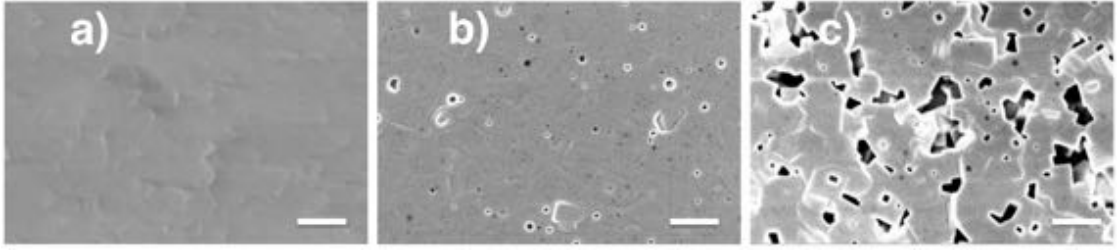
Figure 16: *SEM images of bromide perovskite films spincoated from a saturated precursor solution in DMF with HBr in a 5:1 ratio on a) thiol-functionalized smooth glass, b) amino-functionalized smooth glass and c) amino-functionalized silicon substrates. The side images will still be cropped, but I left them as is for now, so that the scales would be the same. Scale bars - 500 nm.*

5   Conclusion and Outlook

It has been demonstrated that continuous films of organic-inorganic lead bromide perovskite on planar substrates can be achieved using surface silane functionalization and employing the appropriate processing conditions. Adding hydrobromic acid to the the precursor solution was shown to improve the density of nucleation and oriented crystalinity of the film, and new insights were gained on the intermediate behavior of the precursors in solution with HBr. With the addition of hydrogen bromide to a precursor solution in DMF it was also shown that thin continuous films with low surface roughness could be obtained by the addition of a non-solvent during the spincoating process. Alternatively, sequential dropcasting of a saturated precursor solution during a second spincoating step of a perovskite "seed" layer was used to obtain continuous films of controlled crystal size and thickness.

To gain further control over film formation on functionalized substrates a more thorough study of the precise interactions of the silane functional groups with the precursor solutions and perovskite crystals is necessary. The former can be achieved by examining perovskite or lead halide deposition from solvents that coordinate less well with the precursors than DMF or DMSO to check whether the solvent can truly be responsible for screening interaction with the substrate. Moreover, the chemical composition and structure of crystallized intermediates from DMSO

and saturated DMF with HBr could be determined to gain a better insight of why the former caused poor interaction with the silane functional groups and the latter facilitated significantly improved nucleation. The bonding of the perovskite with the functionalized substrate could also be examined using Fourier transform infrared spectroscopy (FTIR) or Raman spectroscopy, and could confirm the hypothesis of thiol binding to the perovskite lead cations, and amine substitution for the organic anions in the perovskite crystal.

Both the non-solvent dripping and sequential deposition methods can also be improved further. For the former the reliability of dripping time needs to be improved, since currently only a very small window of opportunity for obtaining continuous film coverage is present. This could be improved by using a slower spincoating speed, so that the transition between undersaturated and supersaturated is not as sharp, and also by heating the precursor solution before spincoating to increase the supersaturation concentration and facilitate denser nucleation. Xiao et al. also show that larger average crystal size can be achieved by using a solution with a larger dissolved precursor concentration [17]. The sequential deposition method could be significantly improved by finding a reliable method for producing dense films of thin and preferentially oriented crystallites or platelets such as the samples produced with the lead acetate precursor on thiol-functionalized substrates. This would likely yield thin continuous films with low surface roughness.

Since the addition of HBr to the precursor solution was observed to improve density and crystallinity of the resulting films, it might also be beneficial to find a method for incorporating the acid without the addition of water, which was observed to be detrimental to film quality. One possible approach would be to follow a similar method as described by Wang et al. to crystallize $HPbBr_x$, and use it as the lead precursor instead of $PbBr_2$ [27].

Lastly, optoelectronic characterization of the different perovskite films obtained in this study should be performed to determine the fundamental properties of these materials, and their potential for device integration. In particular, the smooth thin films obtained with the non-solvent dripping method could be useful for more reliable determination of the materials optical constants with minimal measurement artifacts from surface inhomogeneities. If the visible improvements in film

quality are accompanied by improvements in optoelectronic properties, bromide perovskites could be deposited on functionalized silicon to produce tandem solar cells, which would be an important step towards high-efficiency, low-cost photovoltaics.

References

[1] M. A. Green, K. Emery, Y. Hishikawa, W. Warta, and E. D. Dunlop, "Solar cell efficiency tables (version 44)," *Progress in Photovoltaics: Research and Applications*, vol. 22, no. 7, pp. 701–710, 2014.

[2] L. Zuo, Z. Gu, T. Ye, W. Fu, G. Wu, H. Li, and H. Chen, "Enhanced photovoltaic performance of ch3nh3pbi3 perovskite solar cells through interfacial engineering using self-assembling monolayer," *Journal of the American Chemical Society*, vol. 137, no. 7, pp. 2674–2679, 2015.

[3] T. Shi, W.-J. Yin, F. Hong, K. Zhu, and Y. Yan, "Unipolar self-doping behavior in perovskite ch3nh3pbbr3," *Applied Physics Letters*, vol. 106, no. 10, pp. –, 2015.

[4] S. Brittman, G. W. P. Adhyaksa, and E. C. Garnett, "The expanding world of hybrid perovskites: materials properties and emerging applications," *MRS Communications*, vol. 5, no. 1, pp. 7–26, 2015.

[5] C. C. Stoumpos, C. D. Malliakas, and M. G. Kanatzidis, "Semiconducting tin and lead iodide perovskites with organic cations: Phase transitions, high mobilities, and near-infrared photoluminescent properties," *Inorganic Chemistry*, vol. 52, no. 15, pp. 9019–9038, 2013.

[6] M. Saba, M. Cadelano, D. Marongiu, F. Chen, V. Sarritzu, N. Sestu, C. Figus, M. Aresti, R. Piras, A. Geddo Lehmann, C. Cannas, A. Musinu, F. Quochi, A. Mura, and G. Bongiovanni, "Correlated electron–hole plasma in organometal perovskites," *Nature Communications*, vol. 5, 09 2014.

[7] N. K. Noel, A. Abate, S. D. Stranks, E. S. Parrott, V. M. Burlakov, A. Goriely, and H. J. Snaith, "Enhanced photoluminescence and solar cell performance via lewis base passivation of organic–inorganic lead halide perovskites," *ACS Nano*, vol. 8, no. 10, pp. 9815–9821, 2014.

[8] T. Salim, S. Sun, Y. Abe, A. Krishna, A. C. Grimsdale, and Y. M. Lam, "Perovskite-based solar cells: impact of morphology and device architecture on device performance," *J. Mater. Chem. A*, vol. 3, pp. 8943–8969, 2015.

[9] G. Cao, "Fundamentals of homogeneous nucleation," in *MSE 502, Sol-Gel Processing [lecture notes]*, University of Washington, 2005.

[10] L. Zhigilei, "Nucleation and growth kinetics," in *MSE 3050, Phase Diagrams and Kinetics [lecture notes]*, University of Virginia, 2013.

[11] K. Reichelt, "Nucleation and growth of thin films," *Vacuum*, vol. 38, no. 12, pp. 1083–1099, 1988.

[12] T.-B. Song, Q. Chen, H. Zhou, C. Jiang, H.-H. Wang, Y. (Michael) Yang, Y. Liu, J. You, and Y. Yang, "Perovskite solar cells: film formation and properties," *J. Mater. Chem. A*, vol. 3, pp. 9032–9050, 2015.

[13] H. B. Kim, I. Im, Y. Yoon, S. D. Sung, E. Kim, J. Kim, and W. I. Lee, "Enhancement of photovoltaic properties of ch3nh3pbbr3 heterojunction solar cells by modifying mesoporous tio2 surfaces with carboxyl groups," *J. Mater. Chem. A*, vol. 3, pp. 9264–9270, 2015.

[14] M. A. Green, A. Ho-Baillie, and H. J. Snaith, "The emergence of perovskite solar cells," *Nat Photon*, vol. 8, pp. 506–514, 07 2014.

[15] J. H. Heo, D. H. Song, and S. H. Im, "Planar ch3nh3pbbr3 hybrid solar cells with 10.4% power conversion efficiency, fabricated by controlled crystallization in the spin-coating process," *Advanced Materials*, vol. 26, no. 48, pp. 8179–8183, 2014.

[16] Q. Chen, H. Zhou, T.-B. Song, S. Luo, Z. Hong, H.-S. Duan, L. Dou, Y. Liu, and Y. Yang, "Controllable self-induced passivation of hybrid lead iodide perovskites toward high performance solar cells," *Nano Letters*, vol. 14, no. 7, pp. 4158–4163, 2014.

[17] Z. Xiao, Q. Dong, C. Bi, Y. Shao, Y. Yuan, and J. Huang, "Solvent annealing of perovskite-induced crystal growth for photovoltaic-device efficiency enhancement," *Advanced Materials*, vol. 26, no. 37, pp. 6503–6509, 2014.

[18] P. Löper, M. Stuckelberger, B. Niesen, J. Werner, M. Filipič, S.-J. Moon, J.-H. Yum, M. Topič, S. De Wolf, and C. Ballif, "Complex refractive index spectra

of ch3nh3pbi3 perovskite thin films determined by spectroscopic ellipsometry and spectrophotometry," *The Journal of Physical Chemistry Letters*, vol. 6, no. 1, pp. 66–71, 2015.

[19] G. Grancini, S. Marras, M. Prato, C. Giannini, C. Quarti, F. De Angelis, M. De Bastiani, G. E. Eperon, H. J. Snaith, L. Manna, and A. Petrozza, "The impact of the crystallization processes on the structural and optical properties of hybrid perovskite films for photovoltaics," *The Journal of Physical Chemistry Letters*, vol. 5, no. 21, pp. 3836–3842, 2014.

[20] S. D. Stranks, P. K. Nayak, W. Zhang, T. Stergiopoulos, and H. J. Snaith, "Formation of thin films of organic–inorganic perovskites for high-efficiency solar cells," *Angewandte Chemie International Edition*, 2015.

[21] M. Liu, M. B. Johnston, and H. J. Snaith, "Efficient planar heterojunction perovskite solar cells by vapour deposition," *Nature*, vol. 501, pp. 395–398, 09 2013.

[22] M. Xiao, F. Huang, W. Huang, Y. Dkhissi, Y. Zhu, J. Etheridge, A. Gray-Weale, U. Bach, Y.-B. Cheng, and L. Spiccia, "A fast deposition-crystallization procedure for highly efficient lead iodide perovskite thin-film solar cells," *Angewandte Chemie*, vol. 126, no. 37, pp. 10056–10061, 2014.

[23] G. E. Eperon, V. M. Burlakov, P. Docampo, A. Goriely, and H. J. Snaith, "Morphological control for high performance, solution-processed planar heterojunction perovskite solar cells," *Advanced Functional Materials*, vol. 24, no. 1, pp. 151–157, 2014.

[24] N. J. Jeon, J. H. Noh, Y. C. Kim, W. S. Yang, S. Ryu, and S. I. Seok, "Solvent engineering for high-performance inorganic–organic hybrid perovskite solar cells," *Nature Materials*, vol. 13, pp. 897–903, 09 2014.

[25] D. T. Moore, H. Sai, K. W. Tan, D.-M. Smilgies, W. Zhang, H. J. Snaith, U. Wiesner, and L. A. Estroff, "Crystallization kinetics of organic–inorganic trihalide perovskites and the role of the lead anion in crystal growth," *Journal of the American Chemical Society*, vol. 137, no. 6, pp. 2350–2358, 2015.

[26] J. M. Frost, K. T. Butler, F. Brivio, C. H. Hendon, M. van Schilfgaarde, and A. Walsh, "Atomistic origins of high-performance in hybrid halide perovskite solar cells," *Nano Letters*, vol. 14, no. 5, pp. 2584–2590, 2014.

[27] F. Wang, H. Yu, H. Xu, and N. Zhao, "Hpbi3: A new precursor compound for highly efficient solution-processed perovskite solar cells," *Advanced Functional Materials*, vol. 25, no. 7, pp. 1120–1126, 2015.

[28] W. Zhang, M. Saliba, D. T. Moore, S. K. Pathak, M. T. Hörantner, T. Stergiopoulos, S. D. Stranks, G. E. Eperon, J. A. Alexander-Webber, A. Abate, A. Sadhanala, S. Yao, Y. Chen, R. H. Friend, L. A. Estroff, U. Wiesner, and H. J. Snaith, "Ultrasmooth organic–inorganic perovskite thin-film formation and crystallization for efficient planar heterojunction solar cells," *Nat Commun*, vol. 6, 01 2015.

[29] Q. Wang, Y. Shao, Q. Dong, Z. Xiao, Y. Yuan, and J. Huang, "Large fill-factor bilayer iodine perovskite solar cells fabricated by a low-temperature solution-process," *Energy Environ. Sci.*, vol. 7, pp. 2359–2365, 2014.

[30] K. Yan, M. Long, T. Zhang, Z. Wei, H. Chen, S. Yang, and J. Xu, "Hybrid halide perovskite solar cell precursors: Colloidal chemistry and coordination engineering behind device processing for high efficiency," *Journal of the American Chemical Society*, vol. 137, no. 13, pp. 4460–4468, 2015.

[31] K. Wojciechowski, S. D. Stranks, A. Abate, G. Sadoughi, A. Sadhanala, N. Kopidakis, G. Rumbles, C.-Z. Li, R. H. Friend, A. K.-Y. Jen, and H. J. Snaith, "Heterojunction modification for highly efficient organic–inorganic perovskite solar cells," *ACS Nano*, vol. 8, no. 12, pp. 12701–12709, 2014.

[32] Y. Ogomi, A. Morita, S. Tsukamoto, T. Saitho, Q. Shen, T. Toyoda, K. Yoshino, S. S. Pandey, T. Ma, and S. Hayase, "All-solid perovskite solar cells with hoco-r-nh3+i– anchor-group inserted between porous titania and perovskite," *The Journal of Physical Chemistry C*, vol. 118, no. 30, pp. 16651–16659, 2014.

Appendices

A   Functionalizing Different Substrates

The following paragraph was initially presented at the beginning of the results section, but had to be reconsidered due to conflicting control samples, as discussed further.

Here the possibility of using surface silane functionalization is demonstrated as an effective tool for controlling perovskite film morphology on different substrates. Figure 17 a), b) and c) shows optical images of the resulting perovskite films on thiol functionalized substrates of smooth glass, plasma etched glass, and silicon respectively. The films were spincoated immediately after dropcasting. Figures 17 d), e) and f) show films produced using the same method, but with a 15 minute loading time before spincoating. With no loading time the nucleation density is significantly better on the etched glass substrate than on the smooth glass and silicon, which is what one would expect on a substrate with larger surface roughness improving the wetting of the perovskite solution. However, when the solution is allowed to sit on the substrate for 15 minutes before spincoating, densities of the three samples become roughly equal, indicating that the thiol-perovskite interaction is relatively slow, but ultimately favorable for denser nucleation. However, the films are still far from being smooth and continuous and the nucleation density increases only marginally with loading time for the etched glass substrate, indicating that, although substrate-perovskite interaction is improved, it is still energetically more favorable for the perovskites to crystallize on themselves than on the substrate. The cubic faceting of the crystals on the substrates with no loading time is also not present in the samples for which the precursor solution was allowed to sit before spinning. This indicates that some type of nucleation - either of the perovskite, or an intermediate configuration in the precursor solution - could be occurring during the loading time, leading to non-preferential templating for further crystal growth.
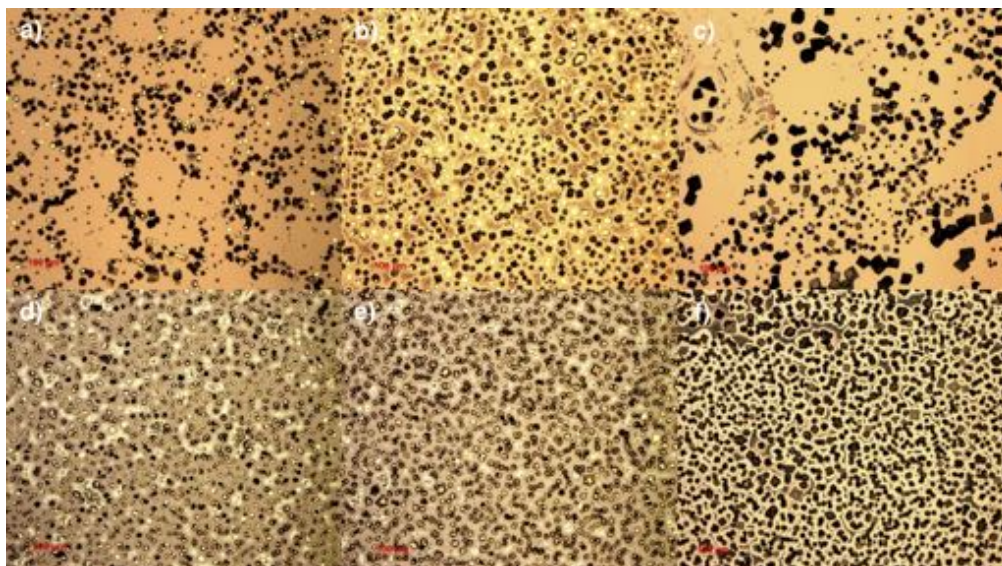
Figure 17: *Optical microscope images of $CH_3NH_3PbBr_3$ films spincoated on thiol-functionalized substrates of a,d) smooth glass, b,e) etched glass and c,f) silicon. Top panels show coverage with no loading time before spinning; bottom panels show coverage with 15 minutes of loading time before spincoating.*

It was initially found that on non-functionalized control samples there was a significant difference in nucleation density between smooth and etched glass substrate, as in panels a) and b) of figure **??**, with some cubic crystallites on both types of substrates. However, when control samples were made again at a later stage in the investigation the results were more similar to the films in panels d) and e) of figure **??** with similar nucleation density and non-faceted crystallites. Thus no valid conclusion could be drawn from the results of figure **??**, since it was not known what caused the sudden change in both morphology and nucleation density in the reference samples. It is possible that this might have been due to the DMF solvent degrading when left in air for a longer time, but this remains to be thoroughly tested.
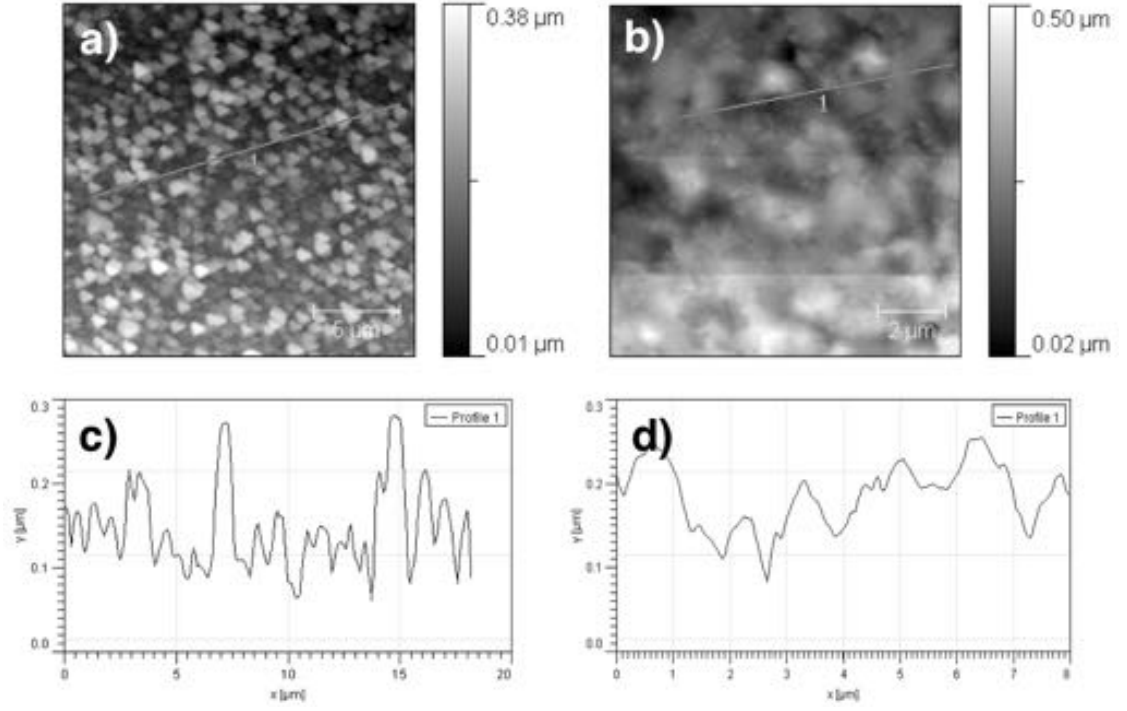
B   Surface Roughness with Toluene Dripping

Figure 18: *AFM images of $CH_3NH_3PbBr_3$ films spincoated with toluene dripping from a) a non-saturated and b) a saturated precursor solution. The triangular features in panel a) are likely due to something attached to the AFM tip, effectively lowering the resolution of the image. The bottom row shows surface profiles corresponding to the line drawn in the overlying AFM images.*

HARALDS ABOLINS

Carolina MacGillavrylaan 1744, Amsterdam, 1098 XE
Tel: 0631335564, haraldsabolins@gmail.com

CURRICULUM VITAE

EDUCATION

Amsterdam University College 2012 – 2015 (Expected)

- **BSc Liberal Arts and Science** (Specialization: Physics)
  - **First year results:** 66 ECP, GPA 3.91/4.00, *Summa Cum Laude*
  - **Second year results:** 69 ECP, GPA 3.88/4.00, *Cum Laude*
  - **Relevant Courses for Capstone Project**
    - Introduction to Chemistry
    - Physics of Heat
    - Statistical Mechanics
    - Quantum Physics
    - Condensed Matter Physics
    - Nanoscience

Riga State Gymnasium No. 1 2006-2012

- **2006 – 2012 Latvian National High School Diploma**
  - Final Grade 9/10
- **2010 – 2012 International Baccalaureate (IB)**
  - Points received 36/45

EXPERIENCE

January 2015 – Present: FOM Institute AMOLF – *Research Intern*

Performing research on perovskite film morphology for photovoltaic applications in the Nanoscale Solar Cells group lead by Dr. Erik Garnett

HARALDS ABOLINS

Carolina MacGillavrylaan 1744, Amsterdam, 1098 XE

Tel: 0631335564, haraldsabolins@gmail.com

June 2014 – Present: Amsterdam University College's Sustainability Association (ASUSA) – *Chair*

Coordination of events, board member activities and decision making process, organization and management of board meetings

September 2014 – Present: Amsterdam University College's Association of Science Students (Curiosity) – *Project Manager*

Responsibility for events and activities relating to applied science, participation in decision-making process during board meetings

September 2013 – June 2014: Amsterdam University College's Sustainability Association (ASUSA) – *Secretary*

Communications with external parties and committee members, event coordination and participation in decision making during board meetings

November 2011 – April 2012: Latvian Samaritan Association – *Volunteer*

Volunteering in irregular events, including food drives and fund-raising events

SKILLS

- Working proficiency with Microsoft Office, LaTeX and Origin
- Working proficiency with Wolfram Mathematica, MATLAB, Python and Racket computing software and programming languages
- Native/Bilingual proficiency in Latvian and English, basic proficiency in French

ONLINE COURSES

- *Learning How to Learn: Powerful mental tools to help you master tough subjects*
  - University of California San Diego Verified Certificate (August 2014)